

VYSOKÉ UČENÍ TECHNICKÉ V BRNĚ
FAKULTA STROJNÍHO INŽENÝRSTVÍ
ÚSTAV MECHANIKY TĚLES,
MECHATRONIKY A BIOMECHANIKY

Ing. František Šebek

**DUCTILE FRACTURE CRITERIA IN MULTIAXIAL
LOADING – THEORY, EXPERIMENTS AND
APPLICATION**

**MEZNÍ PODMÍNKY TVÁRNÉHO LOMU PŘI
VÍCEOSÉM NAMÁHÁNÍ – TEORIE, MĚŘENÍ
A APLIKACE**

Zkrácená verze Ph.D. Thesis

Obor:	Inženýrská mechanika
Školitel:	prof. Ing. Jindřich Petruška, CSc.
Oponenti:	prof. Ing. Petr Horyl, CSc., dr.h.c. doc. Ing. Miroslav Španiel, CSc.
Datum obhajoby:	31. 10. 2016

Klíčová slova

Tvárné porušování, mechanika poškození kontinua, explicitní metoda konečných prvků, kumulace poškození, změkčení materiálu, slitina hliníku.

Keywords

Ductile fracture, continuum damage mechanics, explicit finite element method, damage accumulation, material weakening, aluminium alloy.

Místo uložení práce

Vysoké učení technické v Brně

Fakulta strojního inženýrství

Technická 2896/2

616 69 Brno

Contents

1	Introduction	5
1.1	Motivation	5
1.2	Objectives of the study	5
2	Overview of existing approaches	6
2.1	Phenomenological criteria	6
2.2	Continuum damage mechanics	7
2.3	Void nucleation, growth and coalescence	8
2.4	Porosity based models	8
3	Experiments	8
3.1	Aluminium alloy 2024-T351	8
3.2	Experimental program	10
4	Stress and strain relationship	11
5	Damage accumulation	12
6	Material weakening	14
7	Plasticity	15
7.1	Simulation of tension of smooth cylindrical specimen	16
7.2	Simulations of tension of notched cylindrical specimens	17
7.3	Simulation of tension of notched tubular specimen	17
7.4	Simulation of torsion test	18
7.5	Simulation of upsetting test	19
8	Ductile fracture criterion	19
9	Application of proposed approach	21
9.1	Fracture at axisymmetric tension	21
9.2	Fracture at plane strain tension	22
9.3	Fracture at axisymmetric compression	22
10	Conclusions and future studies	24
10.1	Conclusions	24
10.2	Future studies	24
	References	24
	Curriculum vitæ	29
	Abstract	30

1 Introduction

1.1 Motivation

The problem of ductile fracture in general has become motivating for engineers since *the Industrial Revolution*. With the onset of the industrialization and widespread use of various structural steels and alloys, the problem of fracture has occurred. Bridges and buildings have been constructed from structural steels. The aircraft, automotive, marine, railway and more other engineering fields have started to use metals. It has begun to be challenging to predict fractures in such sectors, especially where human factors and casualties have played a role. Finished products, assemblies, machinery, or structures may be subjected to extreme straining due to accidents, such as train wrecks, traffic collisions, aviation accidents, ship collisions or failures in nuclear or civil engineering. In such cases, it is a great task for engineers to predict the ductile fracture reliably. There is also an amount of forming operations in industrial applications where large plastic deformations occur. Semi-finished products may be subjected to various shaping operations such as bending and twisting, or to forming operations such as forward extrusion, where the fracture is not desirable. On the other hand, material separation processes such as machining, cutting, or trimming – where violating the material integrity is intentional – are applied to semi-finished products before those get the required geometry and properties. Moreover, business competitiveness implies necessity of handling such processes in the most effective way. Therefore, many approaches to ductile fracture [39, 40, 52], more or less complex, have been proposed. However, the literature and experiences reveal the statement that “the more complicated the model, the better the reliability” does not necessarily apply. It may be stated that the more the model is sophisticated, the more expensive is the calibration and the more difficult is the application, which makes such models more academic.

1.2 Objectives of the study

This thesis deals with *the ductile fracture* in the broader sense and does not concern the classical fracture mechanics. In this case, the concept of ductile fracture refers to large plastic energy consuming deformations of ductile polycrystalline metals under monotonic quasi-static loading conditions. *Large plastic deformations* refers to hundreds of percent in the present study. The whole problem is solved from the very beginning when the virgin material is without any damage, although there may be initial amount present. The local approach focuses on a material point where the damage is accumulated. The damage is tracked within the whole solid subjected to straining until the crack initiates and grows. In the final stage of the process, there might be material separation into two or more individual pieces. The number of cracks is not limited and those may occur simultaneously or subsequently in any part of observed solid.

The main goals may be summarized in the following points:

- To theoretically and experimentally study the multiaxial ductile fracture criteria and their application in the scope of Continuum Damage Mechanics (CDM). The main focus deals especially with the experimental program carried out on Aluminium Alloy (AA) 2024-T351 in order to reliably calibrate chosen continuum damage model.
- To conduct the study of nonlinear damage accumulation and its influence on the prediction of the ductile fracture. A special attention is paid to the problem of material weakening and to the estimation of related material constants.
- To discuss the prediction capability and reliability of suggested approaches using verification on existing fracture tests.

2 Overview of existing approaches

2.1 Phenomenological criteria

In the beginnings, phenomenological criteria were developed by engineers who needed to predict the ductile crack initiation and propagation in bulk or sheet metal forming processes. These macroscopically based criteria were relatively simple and with limited usage in the range of stress states in which they were calibrated.

Freudenthal [7] presented energy criterion defining a limiting amount of the plastic work per unit volume. *Cockcroft and Latham* [12] proposed that the crack formation is associated with tensile stress even in predominantly compressive processes. *Brozzo et al.* [17] modified the criterion proposed by Cockcroft and Latham [12] and included the dependence on the mean stress. *Oh et al.* [21] later suggested that it is more reasonable to include just the stress ratio in the model proposed by Cockcroft and Latham [12], so that the model was dimensionless. There are more simple criteria containing only one material constant as these listed above. Those are often called empirical models. Further, the focus will be paid to more sophisticated ones where the crack initiation is predicted by the accumulated damage depending on certain weighting function $\bar{\epsilon}^f$ (state variables), apart from model proposed by Wilkins et al. [22] where the criterion is formulated slightly differently. Macroscopically, fracture occurs when the damage indicator reaches a critical value, the most often unity. Linear incremental relationship between the damage parameter D and equivalent plastic strain $\bar{\epsilon}^p$, when the damage parameter ranges from 0 to 1, may be written as

$$D = \int_0^{\hat{\epsilon}^f} \frac{1}{\bar{\epsilon}^f(\text{state variables})} d\bar{\epsilon}^p, \quad (1)$$

where $\hat{\epsilon}^f$ represents the fracture strain for a given loading path. Damage $D = 0$ denotes the virgin material without any damage while the material experiences a complete loss of ductility and failures when $D = 1$.

Wilkins et al. [22] pointed out that besides the hydrostatic pressure, the deviatoric stress also enhances the damage. The above findings led to the formation of new criteria which concern, apart from the pressure dependence, also the deviatoric stress state dependence. Thus, the equivalent fracture strain is dependent both on the stress triaxiality and on a certain deviatoric stress state parameter. Then, the fracture locus has been most often expressed as an envelope in the space of $(\bar{\epsilon}^f, \eta, \xi)$, where η is the stress triaxiality and ξ is the normalized third invariant of deviatoric stress tensor. *Xue–Wierzbicki model* [39] concerned the Lode dependence through the normalized third invariant of deviatoric stress tensor with the weighting function of damage symmetric with respect to this parameter. *Bai and Wierzbicki* [42] later postulated the asymmetric fracture envelope, not symmetric with respect to the normalized Lode angle.

Extended Mohr–Coulomb criterion [44], based on [1, 3], was expressed through fracture stress at first. Then, it was transformed to strain based space using the metal plasticity with pressure and Lode dependence [42] and Hollomon hardening law [5]. This was the first advanced model including the cut-off. The so-called cut-off represents a threshold of the stress triaxiality below which the damage is not accumulated and fracture does not occur. It should be noted that the major research was focused on the high stress triaxialities in the past. The range of negative stress triaxialities and cut-off have been still the subject of extensive investigations.

Lou *et al.* [45] proposed model with dependence on the stress triaxiality and normalized maximum shear stress. Lou and Huh [49] made an extension considering the stress triaxiality and Lode dependence. Later, Lou *et al.* [52] derived modification considering a changeable cut-off for the stress triaxiality. The weighting function of damage appeared as an asymmetric fracture envelope. *Hosford–Coulomb model* [55, 59] is based on Mohr–Coulomb criterion [1, 3] deployed for fracture. Then, Tresca equivalent stress [2] was substituted by the one proposed by Hosford [16]. Therefore, it was also derived in the stress based form at first. The weighting function of damage was asymmetric with respect to normalized Lode angle after transformation by using Hollomon hardening law.

2.2 Continuum damage mechanics

CDM is based on the macroscopic observation of solid materials. In this case, the constitutive model is coupled with the damage and those influence each other. The degradation process and loss of the load carrying area are due to the irreversible process of void nucleation and growth during straining. This approach represents an alternative to the porosity based models in a phenomenological way. Damage models are often called coupled, compared with phenomenological models which are often called uncoupled. It is because in the case of phenomenological criteria, the damage is influenced by the plasticity but not vice versa.

Kachanov [10] laid the foundations of CDM in the context of creep. He assumed the weakening factor $w = 1$ at the initial moment where there is no damage and that $w = 0$ at the moment of rupture. *Rabotnov* [11] also dealt with creep and suggested that the matrix material degrades through damage parameter D_s which is related to the weakening factor through

$$w = 1 - D_s. \quad (2)$$

Thus, the parameter $D_s = 0$ when there is no damage and $D_s = 1$ when the material experiences the loss of load carrying area. In general, the damage parameter corresponding to reduction of load carrying area may not necessary to be the same as the damage indicator describing the reduction of ductility, thus

$$D_s \neq D. \quad (3)$$

The equivalent matrix stress σ_M is supposed to be greater than the equivalent stress which satisfies the load–displacement curve obtained from experiment, therefore it can be written as

$$D_s \leq D. \quad (4)$$

Xue [40] adopted a material constant β as the weakening exponent, implicating

$$D_s = D^\beta. \quad (5)$$

Finally, the requirement from Equation 4 is satisfied when $\beta \geq 1$.

Lemaitre [30, 31] developed *the concept of effective stress* with respect to isotropic material which emphasizes that the presence of voids raises the effective stress. It was also extended into *the hypothesis of strain equivalence*. *Bonora* [33] presented generally nonlinear damage evolution law which was later extended to the low cycle fatigue [34]. *Børvik et al.* [35] provided ductile damage model for penetration and impact related problems based on constitutive and fracture models proposed by Johnson and Cook [26, 28] and CDM approach introduced by Lemaitre [31]. This model included effects of strain rate and temperature. *Xue* [40, 41] introduced damage plasticity model involving the sensitivity to the hydrostatic pressure and Lode dependence.

2.3 Void nucleation, growth and coalescence

Theoretical research of the void nucleation, growth and coalescence has been mostly performed on the representative volume element containing the void. Such microscopic approach was then used for studying macroscopic behaviour of the complex material containing voids, second phase particles and inclusions.

McClintock [13] assumed the material to contain sets of cylindrical holes of elliptical cross-section where major and minor directions of the applied stresses were parallel with their axes. *Rice and Tracey* [14] studied the growth of a spherical void for a simple tensile remote field. *Le Roy et al.* [23] followed up on the work of Rice and Tracey [14] and developed it further, allowing the change of void shape. However, these efforts were rather theoretical. *RTCL* [36] is a criterion combining model proposed by Rice and Tracey [14] for high stress triaxialities and model proposed by Cockcroft and Latham [12] for intermediate and low stress triaxialities. Here, the model proposed by Rice and Tracey was a modified version derived by Fischer et al. [32]. The model proposed by Cockcroft and Latham given here was derived with the use of von Mises yield criterion, assuming the plane stress state in a certain plane and with neglecting certain shear stress components [36].

2.4 Porosity based models

Porosity based models differ from those mentioned above. These stand on similar theoretical background as previous microscopic approach, but do not accumulate the damage separately from yielding. Instead, it is assumed that the material is porous containing isolated spherical or cylindrical voids at microscopic level and the influence of such voids is incorporated in constitutive framework, instantly affecting the plastic flow.

Gurson [18, 19, 20] laid foundations of the widespread porosity based model and assumed idealized matrix as a perfectly rigid plastic material obeying von Mises yield criterion. The approximate upper bound yield function for volumetrically symmetric deformations around a single spherical void contained the void volume fraction as a key damage parameter. *Tvergaard and Needleman* [24, 25, 27] provided well-known modification of the model proposed by Gurson [18, 19, 20], the so-called GTN model, due to predicting the complete loss of material load carrying capacity at unrealistic level. Previous modification was followed by many others and the model has been still in scope of many researches. It was shown that Lode dependence needs to be introduced to improve the predictive capability and accuracy in shear dominant loading conditions [51, 54].

3 Experiments

3.1 Aluminium alloy 2024-T351

All experiments were conducted on AA 2024-T351. This Al–Cu–Mg alloy, which was solution heat treated, stress-relieved stretched and then cold worked, has face-centred cubic structure and is widely used in aviation and aerospace engineering, among others, for various components because of its high strength to weight ratio and good fatigue resistance. The chemical composition of the particular supplied alloy is given in Table 1. It was obtained by glow discharge optical emission spectroscopy on Spectramat GDS 750. The results are averages from three measurings.

Table 1: Chemical composition of AA 2024-T351.

Element	Si	Fe	Cu	Mn	Mg	Cr	Zn	Ti	Ni
Volume [Weight %]	0.07	0.25	4.3	0.52	1.71	0.00	0.01	0.04	0.00

The material was supplied as a cold rolled plate of metal with dimensions $1500 \times 1000 \times 20$ mm as depicted in Cartesian coordinate system xyz in Figure 1.

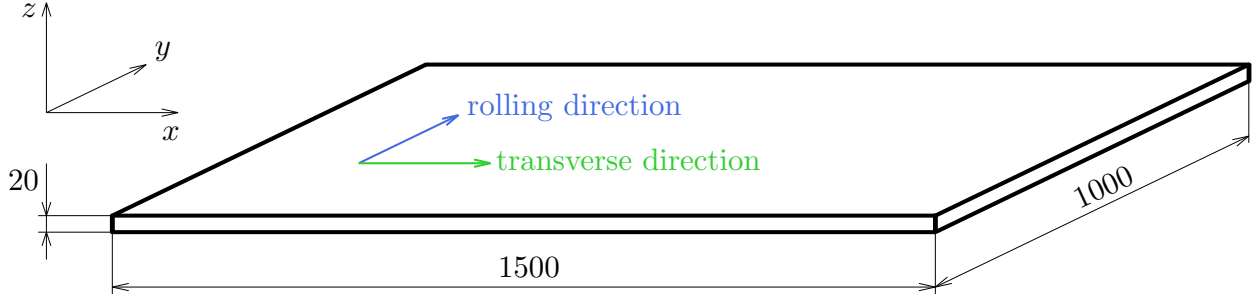


Figure 1: Detailed drawing of supplied plate of aluminium alloy (dimensions in mm).

Specimens, taken in two transverse directions x and y , respectively, were polished and etched for metallographic analysis. The rolling¹ and transverse directions, depicted in Figure 1, were estimated from the size and orientation of grains shown in Figure 2. The rolling direction was studied by fractography using scanning electron microscope, Tescan LYRA3 XMH equipped by Oxford Instruments with energy dispersive X-ray spectroscopy analyser, through secondary and backscattered electrons. Transcrystalline ductile fracture, or the so-called dimpled rupture, governed mostly by the void nucleation and growth was observed. There was also brittle fracture of present intermetallic particles.

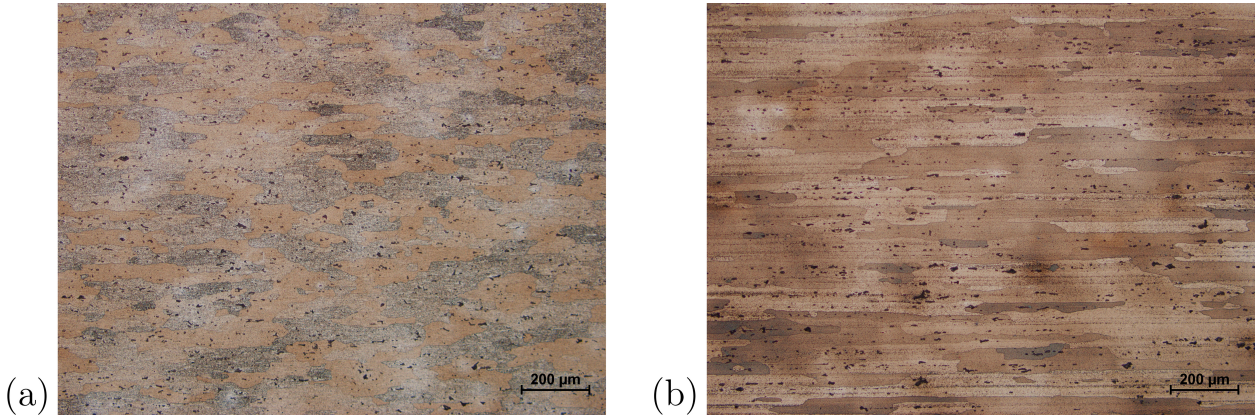


Figure 2: Micrograph of cross-section along: (a) x direction; (b) y direction.

There was significant banding of intermetallic particles for post-mortem specimen from the rolling direction. There was observed only moderate banding of intermetallic particles in case of x direction which is consistent with assumption that this is the direction transverse to rolling. There was also notable omni-directional particle cracking in case of fracture surface from transverse direction.

¹Also called longitudinal direction in the present study.

3.2 Experimental program

In order to obtain *the flow curve* for description of material plastic flow, as well as to calibrate *the fracture model*, there was an experimental program designed and carried out at a room temperature. There are schematic drawings of chosen specimens in Figure 3, where d_0 is the initial diameter of round bar, d_h is the diameter of the hole, R is the notch radius and h is the height. Basic dimensions and an outline of the designed experimental program are in Table 2.

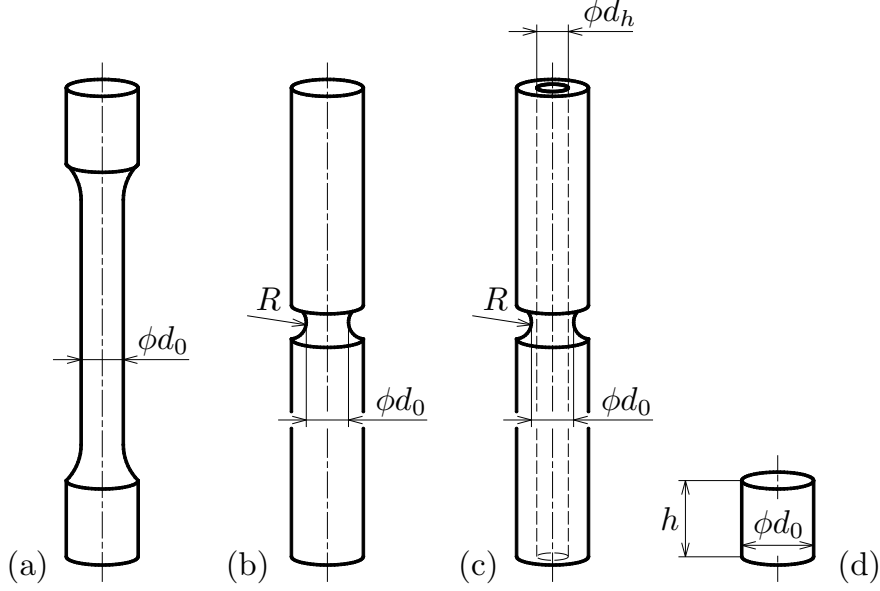


Figure 3: Schematic drawings of specimen types and dimensions used in the experimental program: (a) smooth cylindrical; (b) notched cylindrical; (c) notched tubular; (d) cylindrical.

Table 2: Designed experimental program.

Test	Radial loading condition	Specimen type
1	Tension	Figure 3a, $d_0 = 6$ mm
2		Figure 3b, $d_0 = 9$ mm, R13
3		Figure 3b, $d_0 = 9$ mm, R6.5
4		Figure 3b, $d_0 = 9$ mm, R4
5	Torsion	Figure 3c, $d_0 = 9$ mm, R4, $d_h = 7$ mm
6		Figure 3c, $d_0 = 9$ mm, R4, $d_h = 8$ mm
7	Compression	Figure 3d, $d_0 = 8$ mm, $h = 12$ mm

There are depicted theoretical positions of the fracture tests in the space of the stress triaxiality and normalized third invariant of deviatoric stress tensor in the Figure 4. The geometry of the notched cylindrical specimen with the shallowest notch radius was designed in order to have approximately the same stress triaxiality as the tensile loaded notched tube. The remaining two notched cylindrical specimens with sharper notch radii were designed in order to keep approximately the same interval to each other with respect to stress triaxiality.

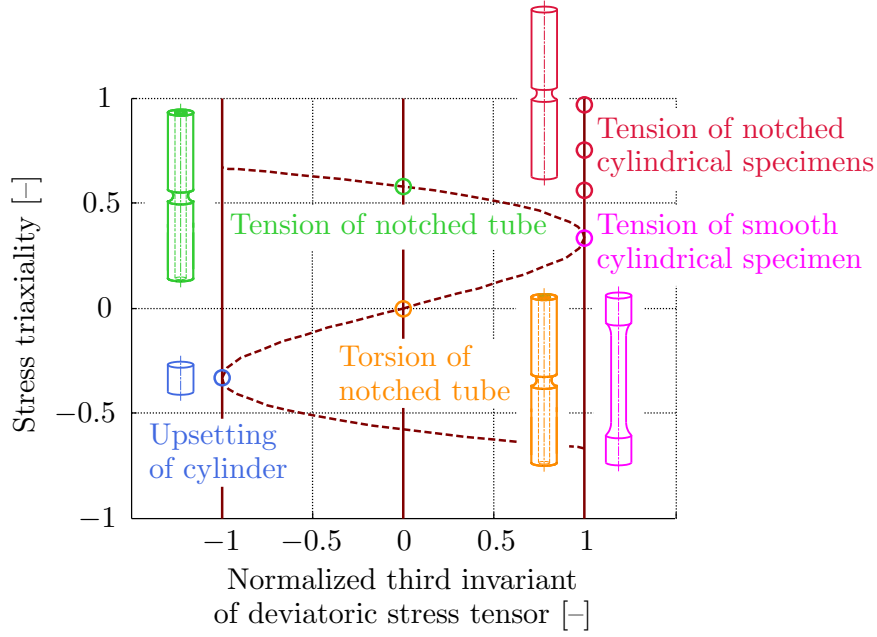


Figure 4: Theoretical positions of the fracture tests in the plane of stress states.

4 Stress and strain relationship

For further work, it is necessary to determine the curve which characterizes the material behaviour and gives the relationship between deformation and stress in a plastically deforming solid. Some other basic mechanical properties of AA 2024-T351 were estimated except for the stress–strain curve. Matrix material was assumed to follow von Mises yield criterion obeying associative flow rule, no matter which plasticity is used further. Nonetheless, it should be assured that the conditions for tensile test of smooth cylindrical specimen are kept the same in further considerations². Additionally, the isotropic hardening was adopted.

Young’s modulus was estimated as $E = 72.5 \text{ GPa}$ by using the engineering curve. The density was estimated as $\rho = 2770 \text{ kg/m}^3$ by using measured dimensions and weight of the reference block of material. Poisson’s ratio was estimated by using density, Young’s modulus and wave velocity. The velocity was measured by using Ultrasonic thickness gauge OLYMPUS 38DL PLUS with contact transducer M110 of 5 MHz. The average value from 5 measuring was $v = 6347 \text{ m/s}$. The wave velocity can be expressed as [15]

$$v = \sqrt{\frac{E}{\rho} \frac{1 - \nu}{(1 + \nu)(1 - 2\nu)}}. \quad (6)$$

Poisson’s ratio was estimated as $\nu = 0.34$ after expressing it from previous equation and solving it within Maple 17.

The tensile test was numerically simulated within the implicit code of Abaqus. Simplified geometry of rectangular coupon of half of the gauge length was used. Mapped mesh was created using a 4-node bilinear axisymmetric quadrilateral elements CAX4R with reduced integration, hourglass control and characteristic size of 0.075 mm. Correct deformation of the specimen was ensured by introducing slight imperfection in the bottom. Hereinafter, the mesh size was based on the study of mesh dependence (convergence) carried out earlier in scope of ductile fracture [42, 60].

²Including the Lode dependence in plasticity.

The extrapolated curve of equivalent stress against equivalent plastic strain³ was determined by using the true curve in multi-linear form by trial and error method, on the basis of comparison of force–displacement curves from experiment and computation until the satisfying match was reached (Figure 5). Then, Swift hardening law was fitted to obtained flow curve by using nonlinear least square method by using the script in MATLAB R2012b. The law takes form [8]

$$\bar{\sigma} = K(\epsilon^0 + \bar{\epsilon}^p)^n, \quad (7)$$

where $\bar{\sigma}$ is the equivalent stress, K is the strength coefficient, ϵ^0 is the reference strain and n is the strain hardening exponent. Fitted material constants were as follows, $K = 788.60$ MPa, $\epsilon^0 = 0.0031$ and $n = 0.1888$. The curve plotted with the use of these constants is depicted in Figure 5b. Force–displacement curves obtained from numerical simulation using the fitted flow curve and the one by using Swift hardening law are compared to the experiment in Figure 5a.

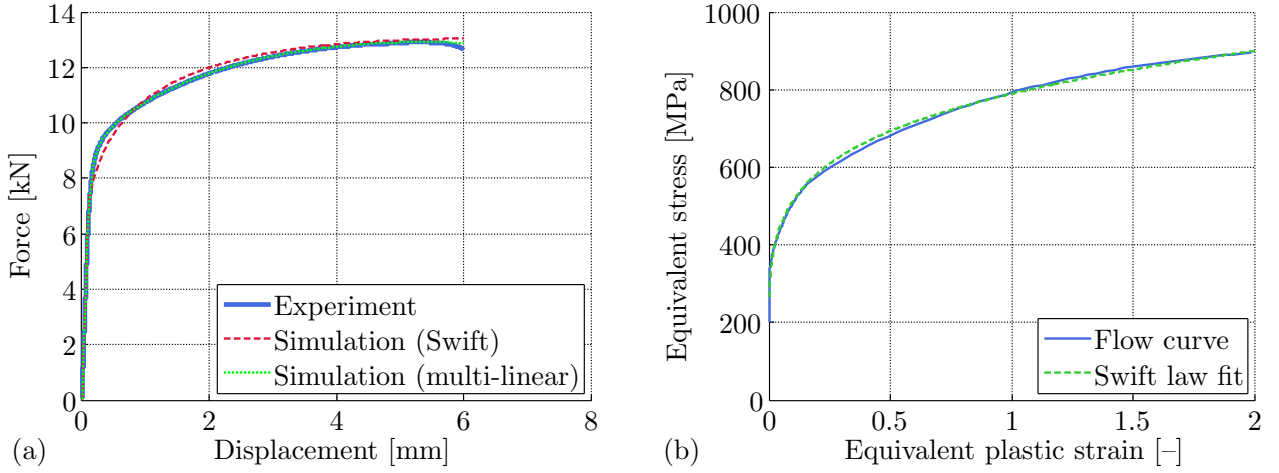


Figure 5: Tensile test of smooth cylindrical specimen: (a) force–displacement curves from experiment and simulations; (b) flow curve and fitted Swift hardening law for AA 2024-T351.

5 Damage accumulation

Miner [6] proposed linear cumulative damage rule on the basis of Palmgren hypotheses [4] in scope of fatigue under variable amplitude loading, the so-called Palmgren–Miner rule. Later, nonlinear damage accumulation was proposed by Marco and Starkey [9], or double damage curve approach by Manson and Halford [29]. Similar approach may be found in ductile fracture related problems. The damage had been assumed as linear function of equivalent plastic strain in the beginnings and it has been considered as nonlinear in the course of time. The damage accumulation, stated as acceleration process analogically to approach of Marco and Starkey [9], which degenerates into linear function when $m = 1$, can be expressed as [40]

$$D = \left(\frac{\bar{\epsilon}^p}{\bar{\epsilon}^f} \right)^m. \quad (8)$$

The greater the damage, the more the material weakens.

³Also called the flow curve.

Xue [40] proposed to derive the damage exponent by using stepwise experiments. Two tensile tests of cylindrical specimens with different stress triaxiality are run until fracture. Then, a larger specimen is pulled onto prescribed deformation, less than the one needed for fracture, the test is interrupted and the deformed specimen is machined into a smaller specimen, inducing different stress triaxiality under tensile loading so that the loading path is changed. Finally, the smaller specimen is pulled until fracture. Stepwise testing was conducted within the present study as well. A notched cylindrical specimen with $d_0 = 9$ mm and $R = 4$ mm (Figure 3b) was used for the first step. A smooth cylindrical specimen with 6 mm diameter (Figure 3a) and certain imperfection was used in the second step. The initial imperfection was used in order to ensure the fracture occurrence in the locus where the root of the notch of previous specimen was. Unfortunately, this approach was found highly unstable and sensitive to input data. Therefore, it is not convenient for the damage exponent calibration in the present form and another technique should be introduced, as described further.

Another method of the damage exponent estimation is to follow the Young's modulus degradation. When \tilde{E} is actual degraded Young's modulus, the concept of effective stress together with strain equivalence hypothesis give [30]

$$D = 1 - \frac{\tilde{E}}{E}. \quad (9)$$

The loading/unloading testing was carried out in order to study the damage evolution. Three smooth cylindrical specimens were loaded in tension and after each 2 % of total engineering strain unloaded and then loaded again. Testing machine Zwick Z250 Allround-Line, tCII, and Zwick multiXtens extensometer were used for the testing with the test speed 1 mm/min, as in most further cases. Values of true plastic strain were subtracted from curves at the moment when the specimens were fully unloaded. Young's moduli were estimated using slopes produced by unloading. Values of damage parameter were calculated by using Equation 9 and plotted against the ratio of true plastic strain to fracture strain in Figure 6b. The fracture strain 0.2346 obtained from numerical simulation conducted in Chapter 4 was used. Experimentally obtained results exhibit linear trend and therefore the power-based model in Equation 8 is not capable to fit the data properly.

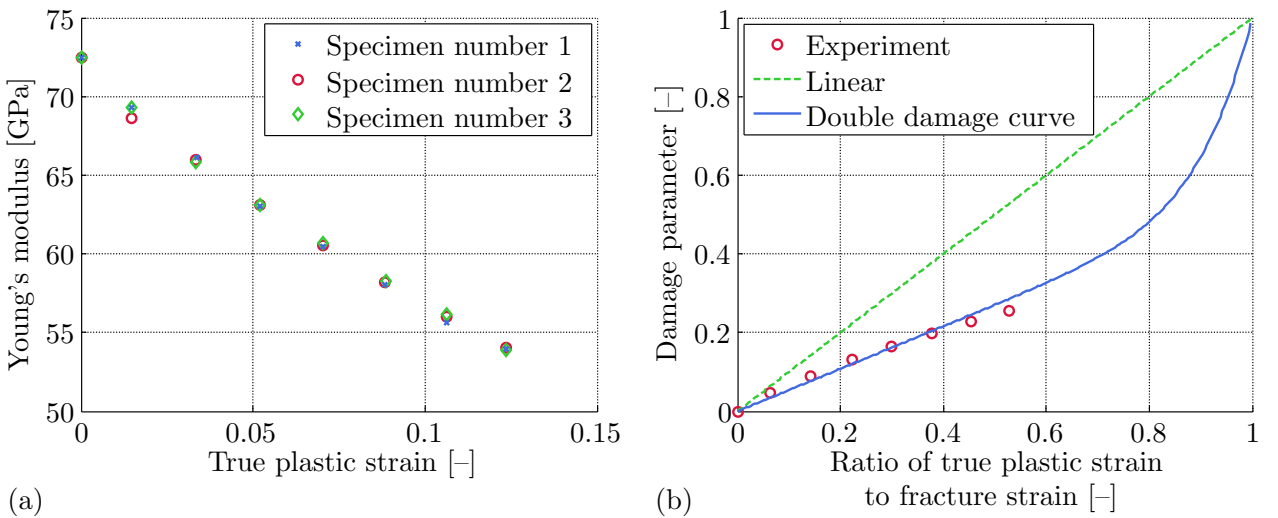


Figure 6: Material degradation of AA 2024-T351 expressed by: (a) measured Young's modulus; (b) calculated damage parameter against the ratio of true plastic strain to fracture strain.

The double damage curve approach introduced by Manson and Halford [29] in scope of cumulative fatigue damage was revisited and applied to ductile fracture here. The damage evolution can be rewritten in the final integral form as

$$D_s = \int_0^{\bar{\epsilon}^f} q_1 \frac{d\bar{\epsilon}^p}{C + \bar{\epsilon}^f} + \int_0^{\bar{\epsilon}^f} q_2(1 - q_1) \left(\frac{\bar{\epsilon}^p}{C + \bar{\epsilon}^f} \right)^{q_2-1} \frac{d\bar{\epsilon}^p}{C + \bar{\epsilon}^f}, \quad (10)$$

with C being explained further. First of all, the slope of initial linear part of damage accumulation was estimated as $q_1 = 0.54$ by using the trial and error method. Then, the second material constant was estimated as $q_2 = 10$ by using the trial and error method again, in order to reasonably extrapolate the damage accumulation to failure (Figure 6b). Presented results are consistent with those obtained by 3D X-ray tomography in scope of micromechanics where the porosity, or void volume fraction and the void density, is related to ductile damage [50].

6 Material weakening

Material weakening is responsible for irreversible microstructural deterioration. It is also governing the coupling of plasticity with fracture model. According to approach proposed by Xue [40, 41], laying the flow curve of matrix equal to conventional flow curve and designating σ_Y as the yield stress, the yield condition may be written as

$$\Phi = \bar{\sigma} - (1 - D_s)\sigma_Y = \bar{\sigma} - (1 - D^\beta)\sigma_Y = 0. \quad (11)$$

The influence of calibrated double damage curve approach together with simple coupling ($\beta = 1$) is depicted in Figure 7a for a tension of the smooth cylindrical specimen until fracture estimated in Chapter 4. The weakening exponent was set as $\beta = 3$ in order to keep the material behaviour unchanged until the proximity of final rupture, among others, to allow to realize the calibration as proposed further. The rapid material deterioration in the end of damage process corresponds to experimental observations and correlates to development of macrocracks in material, leading to violating the structural integrity. However, setting the weakening exponent $\beta = 3$ itself would led in underestimating the force–displacement response from experiment.

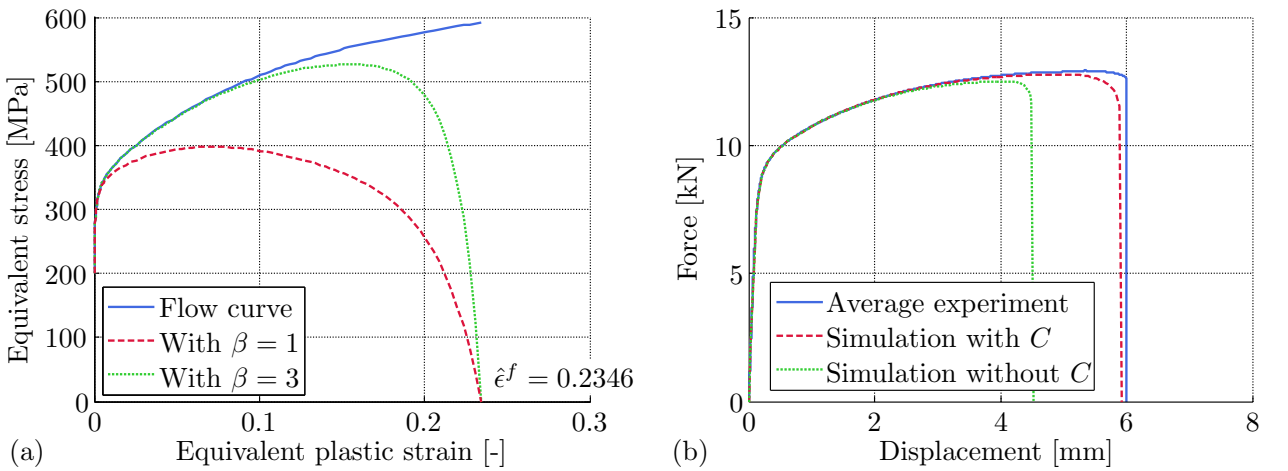


Figure 7: Tensile test of smooth cylindrical specimen after incorporation of damage accumulation and material weakening: (a) in stress–strain curves; (b) in force–displacement responses.

Therefore, there was introduced fracture strain correction coefficient C raising the actual fracture strain (Equation 10). It was calibrated as $C = 0.12$ by the trial and error method until the satisfying match in force–displacement curves was reached (Figure 7b). The simulation of tensile test was performed the same as in Chapter 4 but in explicit code of Abaqus. Vectorized User MATerial (VUMAT) was used for incorporating the double damage curve (damage accumulation) and material weakening.

Basically, the proposed approach combines advantages of both coupled and uncoupled ductile fracture models yielding in the approach similar to *partially coupled models*.

7 Plasticity

All fracture tests were simulated with the use of von Mises yield criterion using the implicit code, as described in Chapter 4. But it was found that force–displacement responses do not match the experiments, so it was necessary to employ more complex plasticity to better describe the material behaviour. It was important because results of these simulations were direct inputs into the ductile fracture model calibration procedure and because the plasticity directly influences the damage accumulation. The critical displacement or twist angle were used in order to indicate the crack initiation by means of sudden decrease of loading. Then, the fracture strain can be obtained from numerical computations together with evolutions of state variables from the crack initiation loci.

The plasticity dependent both on the second and third invariants of deviatoric stress tensor proposed by Kroon and Faleskog [48] was adopted as it preserves the behaviour of uniaxial axisymmetric tension, and also axisymmetric compression which was captured well too, the same as von Mises plasticity which was used for calibration of flow curve and material weakening. Moreover, the yield function is smooth so no singular points on the yield surface have to be treated although it is possible. The yield function with weakening reads

$$\Phi = \bar{\sigma} - (1 - D^\beta) \sigma_Y k, \quad (12)$$

where k is the yield correction function having the form

$$k = 1 - \gamma \omega \left(\frac{1 + \omega_0^{-a}}{\omega^{-a} + \omega_0^{-a}} \right)^a, \quad (13)$$

where γ , ω_0 and a are three material constants and ω is the normalized Lode parameter defined as follows

$$\omega = 1 - \xi^2 = \sin^2(3\theta_L). \quad (14)$$

The yield locus is depicted with calibrated material constants $\gamma = 0.123$, $\omega_0 = 0.18$ and $a = 4$ in Figure 8. The direction of plastic flow is given by an outer normal to the yield surface as

$$\tilde{\mathbf{n}} = \frac{\partial \Phi}{\partial \boldsymbol{\sigma}} = \frac{3 \mathbf{S}}{2 \bar{\sigma}} - 3 \frac{\frac{dk}{d\xi}}{k} \left(2 \frac{3 \mathbf{S}}{2 \bar{\sigma}} \cdot \frac{3 \mathbf{S}}{2 \bar{\sigma}} - \mathbf{I} - \xi \frac{3 \mathbf{S}}{2 \bar{\sigma}} \right), \quad (15)$$

where $\boldsymbol{\sigma}$ is the Cauchy stress tensor, \mathbf{S} is the deviatoric stress tensor and \mathbf{I} is the identity matrix. Previous equation naturally ensures that the stress increment is normal to the yield surface. The differential term in previous equation is following

$$\frac{dk}{d\xi} = 2\gamma \frac{(1 + \omega_0^{-a})^p \omega_0^{-a}}{(\omega^{-a} + \omega_0^{-a})^{a+1}} \xi. \quad (16)$$

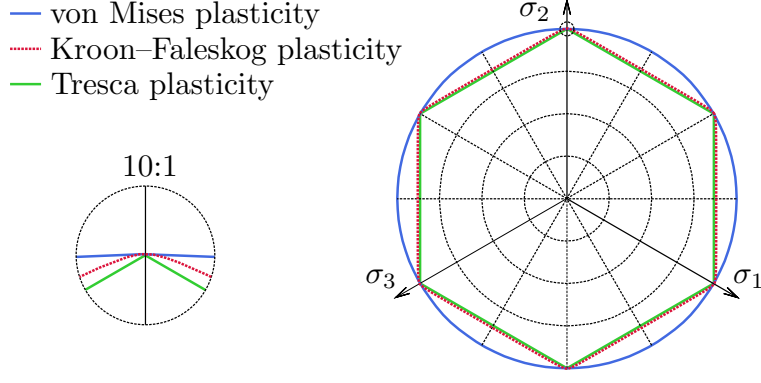


Figure 8: Initial yield loci at a deviatoric plane for AA 2024-T351.

Finally, the plastic multiplier of Kroon–Faleskog plasticity is defined as

$$\dot{\lambda} = \sqrt{\frac{2}{3} \dot{\epsilon}^p : \dot{\epsilon}^p} \left(\sqrt{1 + 9\omega \left(\frac{dk}{d\xi} \right)^2} \right)^{-1}, \quad (17)$$

where $\dot{\epsilon}^p$ is the plastic strain rate tensor. It simplifies to von Mises theory in case of axisymmetry ($\omega = 0$) and generalized shear ($\omega = 1$). The time integration procedure was together with radial return mapping, which satisfies *the Drucker's postulate*, realized according to algorithm described in [40] and implemented in Abaqus time integration scheme using VUMAT.

Simulations of all fracture tests had to be done in order to gain state variables needed in the fracture model calibration. These simulations described in the following sections were done using the explicit code without any influence of the damage accumulation or the material weakening. That is why the weakening effect was set up to affect the properties only in the point close to fracture, so the conditions were similar to the uncoupled approach.

7.1 Simulation of tension of smooth cylindrical specimen

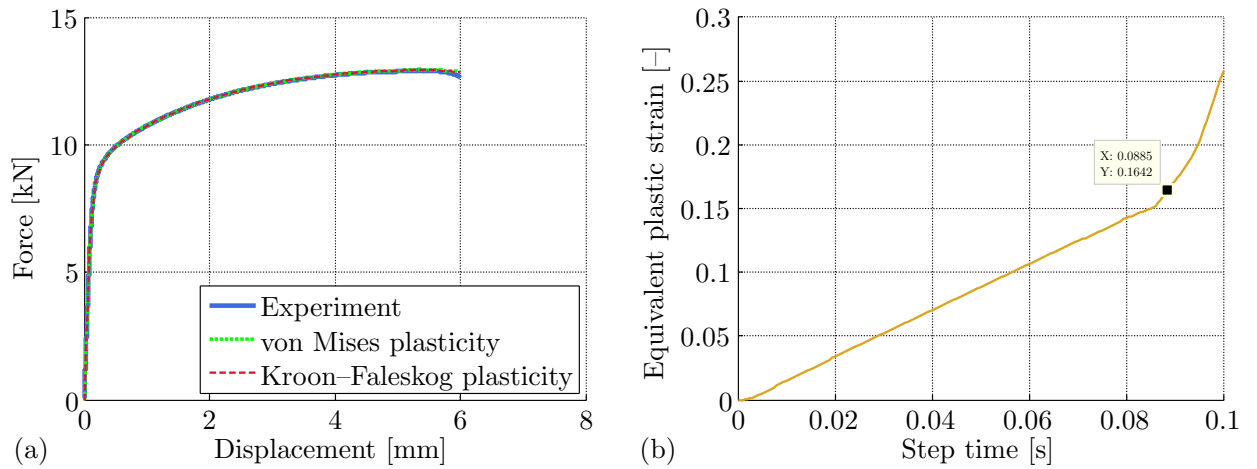


Figure 9: Tension of smooth cylindrical specimen: (a) force–displacement responses of two different plasticities compared to experiment; (b) evolution of the equivalent plastic strain.

Simulation of the tensile test was performed the same as in Chapters 4 and 6. The vertical displacements of bottom edge were constrained and particular displacements were prescribed to upper edge of the model. There is force–displacement response from computation compared to experiment in Figure 9a. The von Mises plasticity did not differ in comparison to Kroon–Faleskog one as expected.

Rapid growth of equivalent plastic strain rate is evident after the necking (Figure 9b), which was minor in case of smooth specimen. Because of this gradient, results are not reliable therefore the specimen was omitted from the ductile fracture calibration.

7.2 Simulations of tension of notched cylindrical specimens

All simulations were realized analogically to those in Chapters 4 and 6. Experimentally obtained force–displacement responses are compared to computationally obtained ones in Figure 10a for both von Mises and Kroon–Faleskog plasticities. The loci were at axes in the notch region where cracks initiated for obtaining state variables. These were chosen to be stress triaxiality and normalized third invariant of deviatoric stress tensor (Figure 10b). Hereinafter, history of those variables are not given for von Mises plasticity but only for Kroon–Faleskog one.

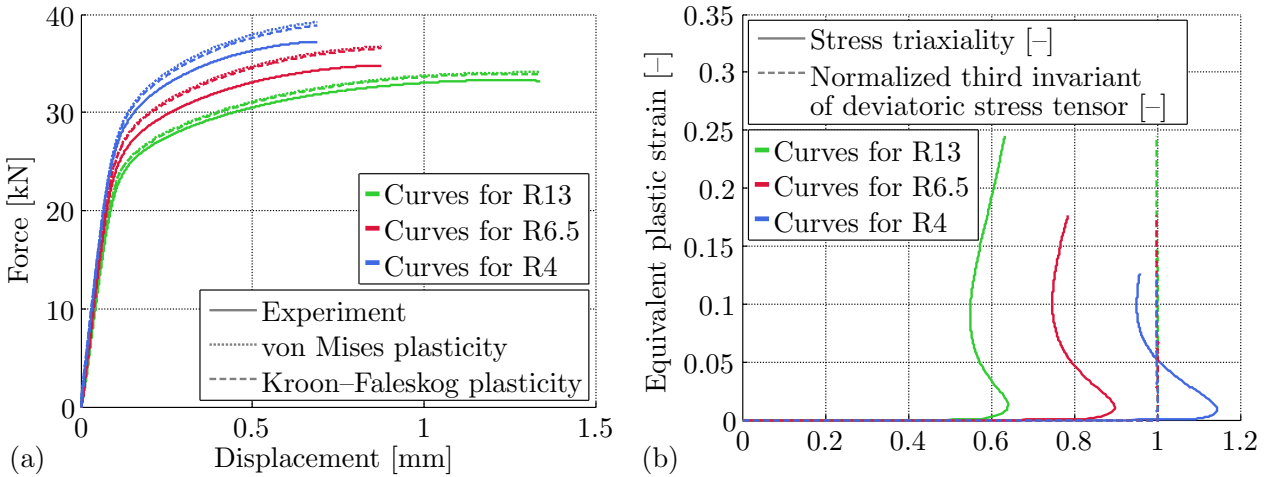


Figure 10: Tensile notched specimens: (a) force–displacement responses from experiments and simulations; (b) evolution of stress triaxialities and normalized Lode angles during loading.

7.3 Simulation of tension of notched tubular specimen

This simulation was performed basically the same as in previous cases of notched cylindrical specimens. The axisymmetric geometry was modelled as the half of specimen. Force–displacement responses from computations and experiment are compared in Figure 11a. The locus for obtaining state variables (Figure 11b) was approximately in the middle of the wall thickness at the notch region. It was found exactly as a locus where normalized Lode angle was close to zero and the stress triaxiality was maximal. The crack was expected to initiate there, because there is a loss of ductility with increasing stress triaxiality [14] and also when moving from axial symmetry to plane strain [39]. This is consistent with results of tension tests of other tubular specimens in literature [47].

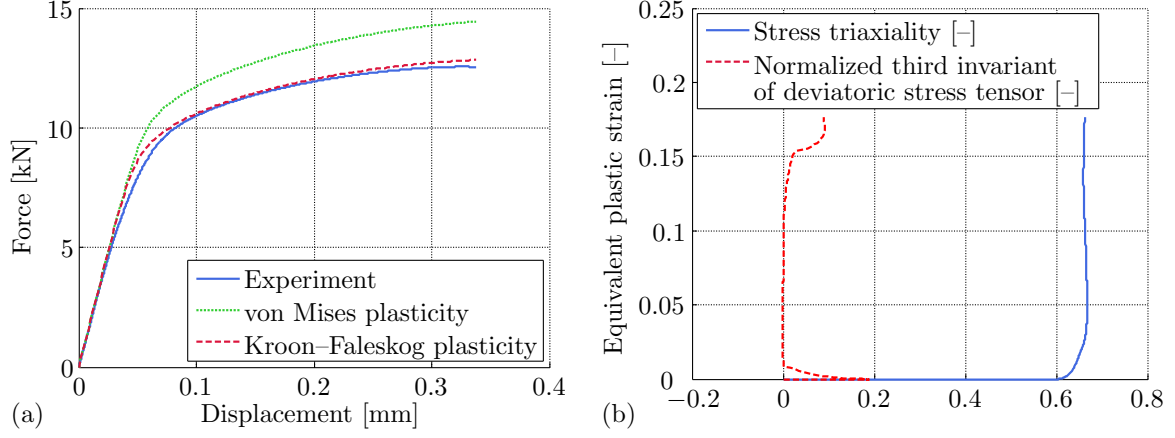


Figure 11: Tensile tubular specimen: (a) force–displacement responses from simulations and experiment; (b) evolution of stress triaxiality and normalized Lode angle during loading.

7.4 Simulation of torsion test

This is the only case when the computational models were not same for the simulations concerning von Mises and Kroon–Faleskog plasticities. An axisymmetric case with twist was used in implicit code, while a three dimensional model was used in case of explicit. The axisymmetric model including twist for simulation concerning von Mises plasticity led to huge time saving. It was meshed with a 4-node generalized bilinear axisymmetric quadrilateral CGAX4R elements with reduced integration, hourglass control, twist and size of 0.075 mm. The three dimensional model was discretized with C3D8R 8-node linear brick elements with reduced integration and hourglass control. These had characteristic size of 0.075 mm in the region of the notch and 0.2 mm in the upper tubular part. The geometry was modelled as the half. The height of the model was only 5 mm because no extensometer was employed. The specimen was designed so as the whole straining took place only in the region of the notch. Therefore, there was no need to model larger section of the upper part which also saved some computational time. The twist was introduced through the reference point on the axis to which the degrees of freedom regarding the twist of the upper surface were coupled. The axial displacement and twist of bottom surface were constrained.

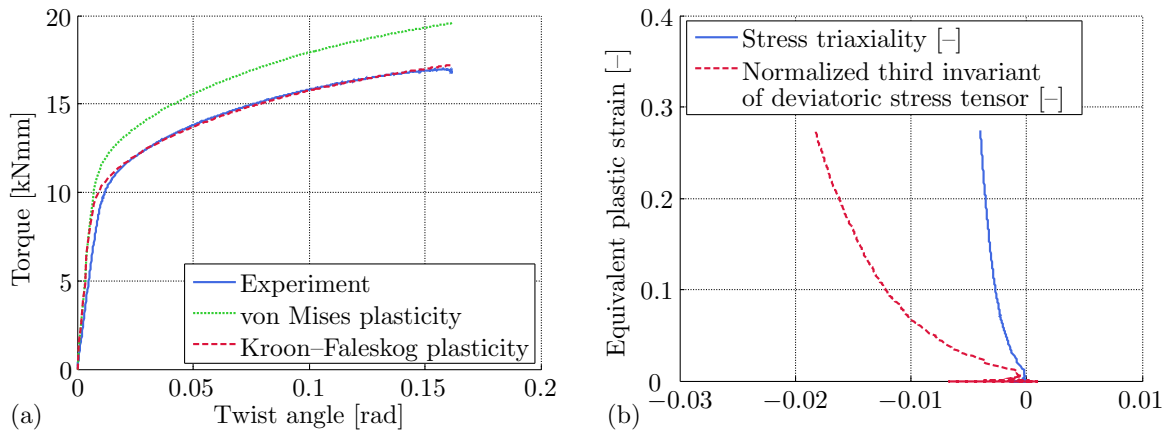


Figure 12: Torsional tubular specimen: (a) torque–twist angle responses from simulations and experiment; (b) evolution of stress triaxiality and normalized Lode angle during loading.

Semi-automatic mass scaling was deployed to target time increment of $1 \cdot 10^{-7}$ s to save computational time. The time increment for most critical elements was approximately $2.7 \cdot 10^{-9}$ s when the mass scaling was not accounted for. The kinetic energy was compared to the internal one in order to ensure there were negligible dynamic effects.

The torque–twist angle responses from simulations compared to experimental observation are depicted in Figure 12a showing very good conformity. The locus for obtaining state variables (Figure 12b) was naturally on the outer surface in the smallest cross-section of the notch. Note the scale of horizontal axis which suggests that the loading was almost perfectly proportional.

7.5 Simulation of upsetting test

The simulation of upsetting test was performed as an axisymmetric case, again, and the specimen was discretized respecting that. Punches with 8 mm radii, of which the size did not represent a reality, were meshed with 0.075 mm RAX2 2-node linear axisymmetric rigid links. The friction coefficient between punches and specimen was identified as 0.05 by trial and error method until the deformations (bulging or barrelling and visible stick and slip regions on upper and bottom surfaces) from simulation matched the experiments. The force–displacement curves from simulation and experiment are depicted in Figure 13a. Similarly as in axisymmetric tension, the Kroon–Faleskog plasticity deviated negligibly from von Mises yield criterion. Stress triaxiality and normalized Lode angle (Figure 13b) were obtained from the surface node in the middle of cylinder height. The loading paths show approximate proportionality corresponding to small amount of friction.

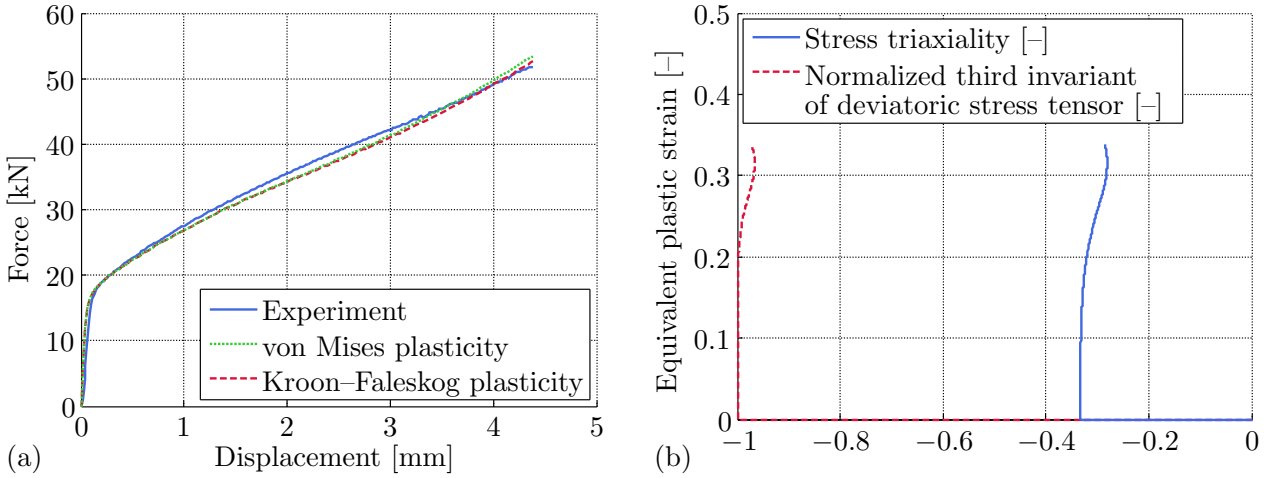


Figure 13: Upsetting test of cylindrical specimen: (a) force–displacement curves from experiment and simulations; (b) loading paths given by stress triaxiality and normalized Lode angle.

8 Ductile fracture criterion

The essential part of ductile fracture model is its fracture envelope defined by weighting function of damage. Besides the fracture strain, stress triaxiality and normalized third invariant of deviatoric stress tensor are inputs into the ductile fracture calibration. There are two possible calibration techniques. The one used in the present thesis is based on the averaging of two latter mentioned state variables. The averaging is then based on adopted damage rule.

With respect to Equation 10, the above mentioned approach for average stress triaxiality is

$$\eta_{av} = \frac{q_1}{\hat{\epsilon}^f} \int_0^{\hat{\epsilon}^f} \eta \, d\bar{\epsilon}^p + \frac{q_2(1-q_1)}{\hat{\epsilon}^f} \int_0^{\hat{\epsilon}^f} \eta \left(\frac{\bar{\epsilon}^p}{\hat{\epsilon}^f} \right)^{q_2-1} d\bar{\epsilon}^p, \quad (18)$$

with analogical formula for average normalized third invariant of deviatoric stress tensor ξ_{av} .

The KHPS2 (Kubík Hůlka Petruška Šebek 2) criterion [53], rising from KHPS (Kubík Hůlka Petruška Šebek) criterion [53], was chosen on the basis of good approximation ability, which is partly at the expense of material constants amount, and presence of cut-off in reasonable level. The asymmetric weighting function of damage with respect to normalized third invariant of deviatoric stress tensor can be written as follows

$$\bar{\epsilon}^f(\eta, \xi) = \left[\frac{1}{2} \left(\frac{G_4}{\langle \eta + g \rangle} + \frac{G_5}{\langle \eta + g \rangle} \right) - \frac{G_6}{\langle \eta + g \rangle} \right] \xi^2 + \frac{1}{2} \left(\frac{G_4}{\langle \eta + g \rangle} - \frac{G_5}{\langle \eta + g \rangle} \right) \xi + \frac{G_6}{\langle \eta + g \rangle}, \quad (19)$$

where G_1, \dots, G_6 are six material constants and g is a parabolic function governing the cut-off beyond which the damage is not accumulated. It reads

$$g(\xi) = \left(G_3 + \frac{G_1 - G_3}{2} - G_2 \right) \xi^2 + \frac{G_1 - G_3}{2} \xi + G_2. \quad (20)$$

The criterion calibration was realized by MATLAB script. The final set of calibrated constants was $G_1 = -0.178$, $G_2 = 1.195$, $G_3 = 1.189$, $G_4 = 0.104$, $G_5 = 0.301$ and $G_6 = 0.327$. Calibrated fracture envelope with its cut-off plane is depicted in Figure 14a where red circles correspond to tensions of notched cylindrical specimens, the magenta diamond to torsion test, the magenta hexagram to tension of notched tubular specimen and the blue square to compression. The envelope is also depicted in the space of principal plastic strains ($\epsilon_I, \epsilon_{II}, \epsilon_{III}$) and stress triaxiality (Figure 14b).

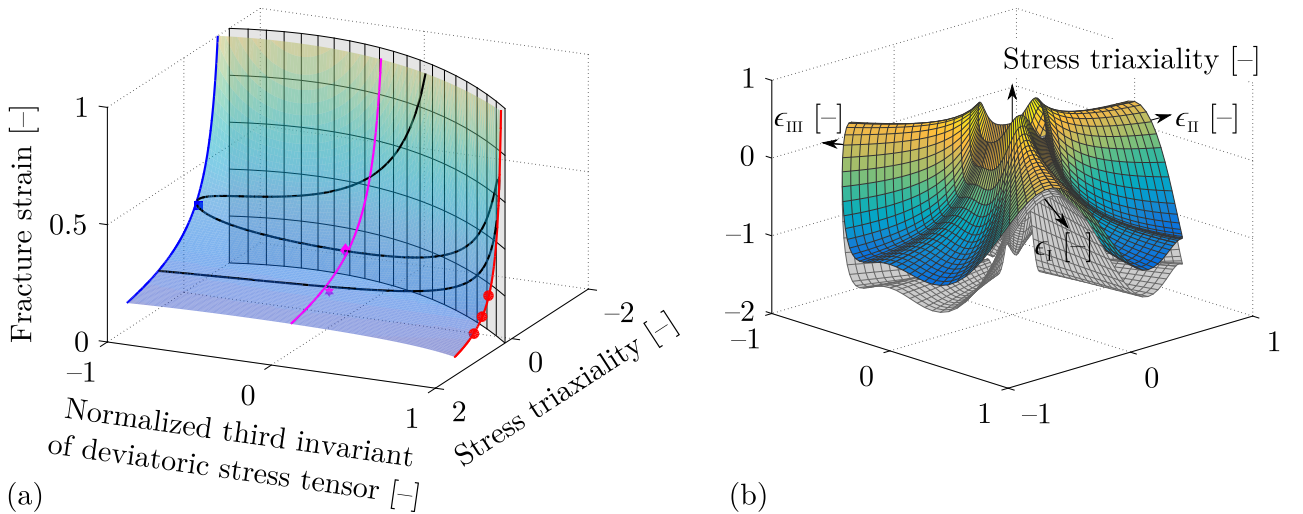


Figure 14: Calibrated fracture envelope of KHPS2 criterion for AA 2024-T351 in the space of: (a) fracture strain and state variables; (b) principal plastic strains and the stress triaxiality.

9 Application of proposed approach

The developed approach was applied to conducted fracture tests to show the prediction ability and reliability. It is always good to verify what has been calibrated and it should not be otherwise in the case of ductile fracture models. Three tests have been chosen, one of each specific stress state, the axisymmetric tension of notched cylindrical specimen, plane strain tension of notched tubular specimen and axisymmetric compression of cylinder. Attention was paid to overall description of the fracture in force–displacement responses as well as in prediction of crack initiation locus and its propagation.

9.1 Fracture at axisymmetric tension

The tensile test of notched cylindrical specimen with R13 notch radius should be closest to the one of smooth cylindrical specimen, towards which the whole approach was basically calibrated. Therefore, it should exhibit very good match with experimental observation.

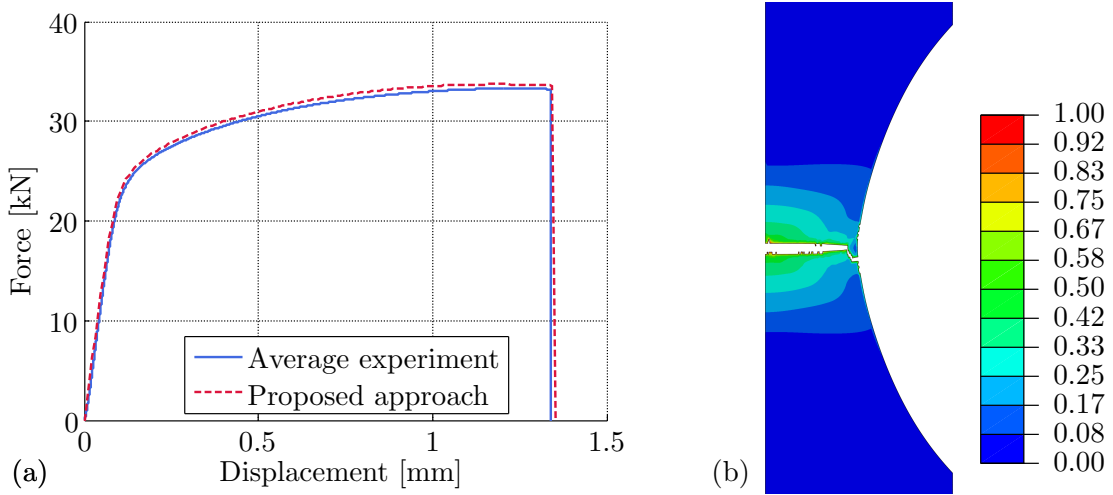


Figure 15: Tensile test of notched cylindrical specimen with R13 notch: (a) force–displacement responses from simulation and experiment; (b) field of damage parameter after the separation.

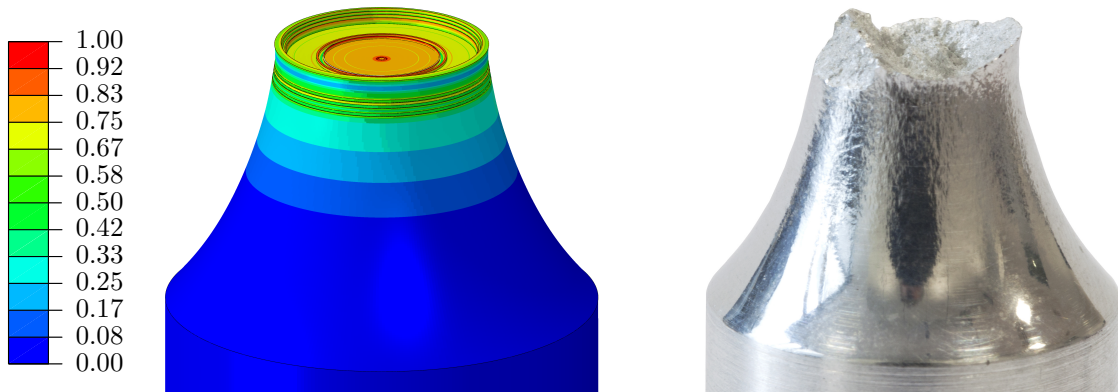


Figure 16: Field of damage parameter of one half of swept model of notched cylindrical specimen with R13 notch radius and one half of post-mortem specimen after the tensile test.

The simulation was replicated in the same way as in Section 7.2 with the difference that the specimen was not modelled as axisymmetric half, but as axisymmetric whole, so the crack propagation could be performed without being influenced by boundary conditions. There is a force–displacement response from computation compared to experimental one in Figure 15a with an excellent match, as expected. The crack initiated on the axis and propagated horizontally at first. It was followed by the slant fracture in a final stage (Figure 15b). The fracture surface was also swept to be compared with experiment in detail. Round specimens did not show perfect cup and cone fracture but still, there was apparent slant fracture in the final stage which is in good correspondence with computation (Figure 16).

9.2 Fracture at plane strain tension

Tension at plane strain should have produced the slant fracture as in the case of the notched tube. The simulation was replicated in the same way as in Section 7.3. The only difference was modelling whole axisymmetric specimen, in order to not influence the fracture by boundary conditions. There are force–displacement responses from computation and experiment which are very close, only the final fracture was slightly over predicted as shown in Figure 17a. The crack initiated approximately in the middle of the specimen thickness at the notch region as assumed already in Section 7.3 during obtaining state variables for calibration procedure. It propagated horizontally, which is unfortunately in contradiction with experimental observations.

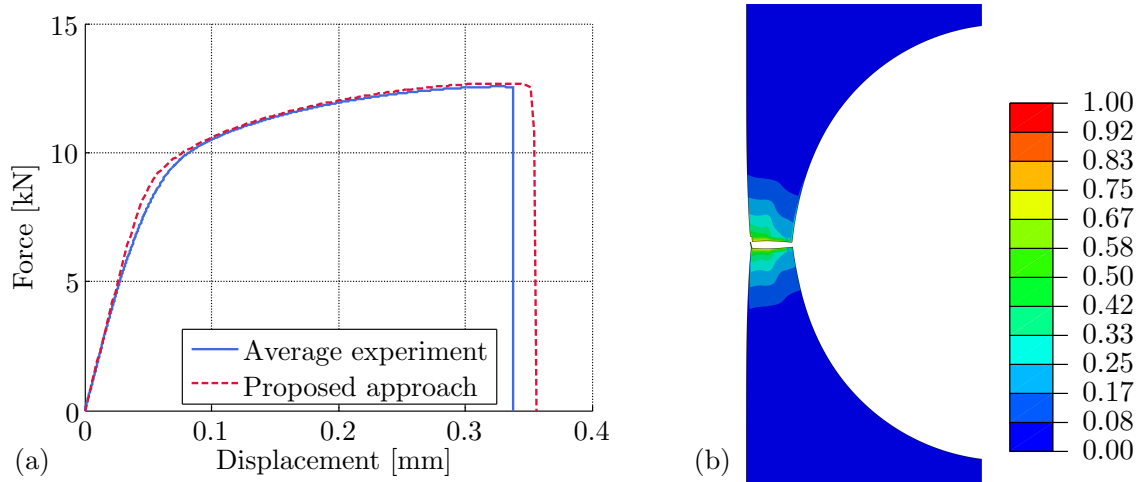


Figure 17: Tensile test of notched tubular specimen: (a) force–displacement responses from simulation and experiment; (b) field of damage parameter after the specimen separation.

9.3 Fracture at axisymmetric compression

In the end, the upsetting test was investigated. The simulation was replicated as in Section 7.5 but in three dimensional space. The cylinder was discretized by mapped mesh with 8-node linear bricks C3D8R with reduced integration, hourglass control and characteristic size of 0.075 mm. Punches were meshed with R3D4 bilinear rigid quadrilateral 4-node three dimensional elements with the same size as the cylinder. The semi-automatic mass scaling was also deployed to target time increment of $1 \cdot 10^{-7}$ s while the time increment for most critical elements were approximately $3.35 \cdot 10^{-9}$ s without accounting for mass scaling. The kinetic energy was checked with respect to internal one to ensure negligible dynamic effects.

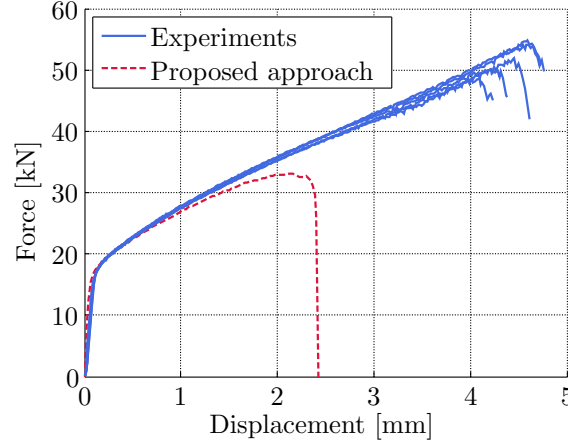


Figure 18: Force responses of compressed cylinders from simulation and experiments.

Force-displacement responses from experiments are compared to computation in Figure 18. The simulation grossly underestimated the reality, because the initiation was in the centre of the specimen, whereas the equivalent plastic strain was much higher than the one on the outer surface (0.7 compared to 0.2) from which the fracture model was calibrated. Xue [43] also reported that there was higher equivalent plastic strain in the centre of cylinder but the crack did not initiate there. Instead, it initiated in the corners of the specimen and propagated diagonally to the centre. Such behaviour was also observed experimentally [40]. Despite that, the fracture model was conventionally calibrated from the outer surface in the middle of the specimen height as in [37]. It is not possible to extract state variables from specimen corners which come into contact with punches and where the results are distorted. On the other hand, the proposed model was able to perform the slant fracture as in experiment at least (Figure 19).

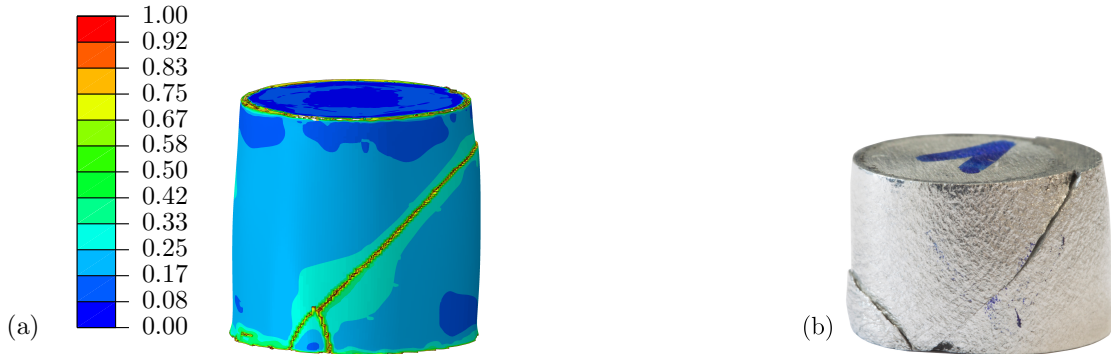


Figure 19: The compression test: (a) field of damage parameter obtained from numerical simulation on a computational model; (b) cracked cylindrical specimen after the experiment.

The upsetting test has been still used for ductile fracture calibration [46], while not many authors provide information about the locus used for obtaining the state variables. The specimen is not convenient for the calibration because of problems with obtaining relevant data from the computation. There are circumstances under which the crack might initiate from the outer surface. Those correspond to compression of very ductile metals or with dry friction conditions yielding in high barreling and nonnegligible tensile circumferential stresses on the outer surface [56]. Then, cracks might even be vertical. But such cases are tried to be omitted within the calibration of ductile fracture because of high nonproportionality of the loading.

10 Conclusions and future studies

10.1 Conclusions

This paragraph summarizes the achieved goals. The approach was outlined after the careful study of literature. Experiments were designed using several geometries in order to capture various stress states. The whole experimenting was performed on the 2024-T351 aluminium alloy. The damage accumulation could be studied by using stepwise experimenting. Unfortunately, it was revealed that this was not reliable to prove the nonlinear damage accumulation due to high sensitivity on input parameters. Therefore, alternative way in the form of loading/unloading was carried out. Sequentially, the double damage curve approach was revisited and material weakening related constants were estimated. The Kroon–Faleskog plasticity and KHPS2 phenomenological ductile fracture criterion were calibrated using scripts created in MATLAB. These models were coupled via the inclusion of the softening effect. Then, proposed methodology was applied to existing fracture tests in order to verify them, using the implemented VUMAT user subroutine within the commercial explicit finite element code Abaqus version 6.14.

The problem had arisen in compression testing. It was revealed that the upsetting test of simple cylinder is not suitable for calibration of ductile fracture criteria. It is due to questionable locus of crack initiation which is compounded by the presence of friction. It is obvious that the point representing the compression in space of $(\bar{\epsilon}^f, \eta, \xi)$ is not correct. It is supported by the location of tensile tests of cylindrical specimens suggesting that the curve corresponding to $\xi = -1$ should have been positioned towards higher fracture strains. Then, the fracture envelope would have formed more curved shape. It would be convenient to have two experiments on axisymmetric compression condition et least.

The approach seems to be promising, but it should be validated by conducting a broader experimental campaign with more extensive computing, of course.

Finally, it can be concluded that all the outlined goals were fulfilled.

10.2 Future studies

The obtained results imply the connection between monotonic and cyclic loading. The ultra low cycle fatigue poses together with monotonic loading the space for further study. There is certainly a smooth transition between these two phenomena. There is definitely potential in finding a unified approach to those problems, but even if the extension to or coupling with fatigue might be challenging, it has still seemed to be long term.

The damage accumulation also needs further investigation. This might be realized using techniques such as the X-ray microtomography and there is a room for ultrasound or DIC measurement as well.

Negative stress triaxialities and cut-off region are worthy of future studies. It is connected with better description of conditions in compression. This might be comprised by the upsetting of notched cylinder or cylinder with specific recess. Then, there would be more evident locus of ductile fracture initiation. Moreover, more appropriate stress state and loading history might be reached. Another alternative to describe the condition at $\xi = -1$ is in a biaxial tension of a cross-like specimen.

The probabilistic approach to ductile fracture seems to be very interesting in accounting for the deviation in identified strains to fracture [61].

Accounting for reversal loading, precompression, pretension or pretorsion, which seem to play nonnegligible role in ductile fracture [38, 57, 58], might be considered.

References

- [1] COULOMB C. A. Essai sur une application des règles *de maximis & minimis* à quelques problèmes de statique, relatifs à l'architecture. *Mémoires présentés à l'Académie des Sciences*, 1776, pp. 343–384 (in French).
- [2] TRESCA M. H. Mémoire sur l'écoulement des corps solides soumis à de fortes pressions. *Compte Rendu des Séances de l'Académie des Sciences*, 1864, pp. 754–758 (in French).
- [3] MOHR O. Welche Umstände bedingen die Elastizitätsgrenze und den Bruch eines Materials? *Zeitschrift des Vereins deutscher Ingenieure*, 1900, Nr. 45, pp. 1524–1530 (in German).
- [4] PALMGREN A. Die Lebensdauer von Kugellagern. *Zeitschrift des Vereins Deutscher Ingenieure*, 1924, Vol. 68, No. 14, pp. 339–341 (in German).
- [5] HOLLOMON J. H. Tensile deformation. *Metals Technology*, 1945, pp. 268–290.
- [6] MINER M. A. Cumulative damage in fatigue. *Journal of Applied Mechanics*, 1945, pp. A-159–A-164.
- [7] FREUDENTHAL A. M. *The inelastic behavior of engineering materials and structures*. John Wiley & Sons, New York, 1950.
- [8] SWIFT H. W. Plastic instability under plane stress. *Journal of the Mechanics and Physics of Solids*, 1952, Vol. 1, Issue 1, pp. 1–18.
- [9] MARCO S. M., STARKEY W. L. A concept of fatigue damage. *Transactions of the ASME*, 1954, pp. 627–632.
- [10] KACHANOV L. M. Rupture time under creep conditions. *Izvestia Akademii Nauk SSSR, Otdelenie Tekhnicheskikh Nauk*, 1958, No. 8, pp. 26–31 (in Russian).
- [11] RABOTNOV Y. N. On the equations of state for creep. *Progress in Applied Mechanics*, 1963, the Prager Anniversary Volume, pp. 307–315.
- [12] COCKCROFT M. G., LATHAM D. J. Ductility and the workability of metals. *Journal of the Institute of Metals*, 1968, Vol. 96, pp. 33–39.
- [13] MCCLINTOCK F. A. A criterion for ductile fracture by the growth of holes. *Journal of Applied Mechanics*, 1968, Vol. 35, No. 2, pp. 363–371.
- [14] RICE J. R., TRACEY D. M. On the ductile enlargement of voids in triaxial stress fields. *Journal of the Mechanics and Physics of Solids*, 1969, Vol. 17, Issue 3, pp. 201–217.
- [15] DATE E. H. F., ATKINS M., BEATON G. V. Measurement of the elasticity and ultrasound velocities of steel. *Ultrasonics*, 1971, Vol. 9, Issue 4, pp. 209–214.
- [16] HOSFORD W. F. A generalized isotropic yield criterion. *Journal of Applied Mechanics*, 1972, pp. 607–609.
- [17] BROZZO P., DELUCA B., RENDINA R. A new method for the prediction of formability limits in metal sheets. In *Proceedings of the 7th Biennial Conference of the International Deep Drawing Research Group*, Amsterdam, Netherlands, 1972.

- [18] GURSON A. L. *Plastic flow and fracture behavior of ductile materials incorporating void nucleation, growth, and interaction*. Ph.D. Thesis, Brown University, 1975.
- [19] GURSON A. L. *Continuum theory of ductile rupture by void nucleation and growth: Part I - Yield criteria and flow rules for porous ductile media*. Technical Report No. 39, Division of Engineering, Brown University, 1975.
- [20] GURSON A. L. Continuum theory of ductile rupture by void nucleation and growth: Part I—Yield criteria and flow rules for porous ductile media. *Journal of Engineering Materials and Technology*, 1977, Vol. 99, No. 1, pp. 2–15.
- [21] OH S. I., CHEN C. C., KOBAYASHI S. Ductile fracture in axisymmetric extrusion and drawing: Part 2—Workability in extrusion and drawing. *Journal of Engineering for Industry*, 1979, Vol. 101, No. 1, pp. 36–44.
- [22] WILKINS M. L., STREIT R. D., REAUGH J. E. *Cumulative-strain-damage model of ductile fracture: Simulation and prediction of engineering fracture tests*. Technical Report UCRL-53058, Lawrence Livermore National Laboratory, California, 1980.
- [23] LE ROY G., EMBURY J. D., EDWARD G., ASHBY M. F. A model of ductile fracture based on the nucleation and growth of voids. *Acta Metallurgica*, 1981, Vol. 29, Issue 8, pp. 1509–1522.
- [24] TVERGAARD V. Influence of voids on shear band instabilities under plane strain conditions. *International Journal of Fracture*, 1981, Vol. 17, No. 4, pp. 389–407.
- [25] TVERGAARD V. On localization in ductile materials containing spherical voids. *International Journal of Fracture*, 1982, Vol. 18, No. 4, pp. 237–252.
- [26] JOHNSON G. R., COOK W. H. A constitutive model and data for metals subjected to large strains, high strain rates and high temperatures. In *Proceedings of the 7th International Symposium on Ballistics*, The Hague, Netherlands, 1983, pp. 541–547.
- [27] TVERGAARD V., NEEDLEMAN A. Analysis of the cup-cone fracture in a round tensile bar. *Acta Metallurgica*, 1984, Vol. 32, No. 1, pp. 157–169.
- [28] JOHNSON G. R., COOK W. H. Fracture characteristics of three metals subjected to various strains, strain rates, temperatures and pressures. *Engineering Fracture Mechanics*, 1985, Vol. 21, No. 1, pp. 31–48.
- [29] MANSON S. S., HALFORD G. R. *Re-examination of cumulative fatigue damage analysis—An engineering perspective*. NASA Technical Memorandum 87325, 1985.
- [30] LEMAITRE J. Coupled elasto-plasticity and damage constitutive equations. *Computer Methods in Applied Mechanics and Engineering*, 1985, Vol. 51, pp. 31–49.
- [31] LEMAITRE J. A continuous damage mechanics model for ductile fracture. *Journal of Engineering Materials and Technology*, 1985, Vol. 107, No. 1, pp. 83–89.
- [32] FISCHER F. D., KOLEDNIK O., SHAN G. X., RAMMERSTORFER F. G. A note on calibration of ductile failure damage indicators. *International Journal of Fracture*, 1995, Vol. 73, Issue 4, pp. 345–357.

- [33] BONORA N. A nonlinear CDM model for ductile failure. *Engineering Fracture Mechanics*, 1997, Vol. 58, No. 1/2, pp. 11–28.
- [34] BONORA N., NEWAZ G. M. Low cycle fatigue life estimation for ductile metals using a nonlinear continuum damage mechanics model. *International Journal of Solids and Structures*, 1998, Vol. 35, No. 16, pp. 1881–1894.
- [35] BØRVIK T., HOPPERSTAD O. S., BERSTAD T., LANGSETH M. A computational model of viscoplasticity and ductile damage for impact and penetration. *European Journal of Mechanics - A/Solids*, 2001, Vol. 20, Issue 5, pp. 685–712.
- [36] TÖRNQVIST R. *Design of crashworthy ship structures*. Ph.D. Thesis, Technical University of Denmark, 2003, ISBN: 87-89502-74-4.
- [37] BAO Y. *Prediction of ductile crack formation in uncracked bodies*. Ph.D. Thesis, Massachusetts Institute of Technology, 2003.
- [38] BAO Y., TREITLER R. Ductile crack formation on notched Al2024-T351 bars under compression–tension loading. *Materials Science and Engineering: A*, 2004, Vol. 384, Issues 1–2, pp. 385–394.
- [39] WIERZBICKI T., BAO Y., LEE Y.-W., BAI Y. Calibration and evaluation of seven fracture models. *International Journal of Mechanical Sciences*, 2005, Vol. 47, Issues 4–5, pp. 719–743.
- [40] XUE L. *Ductile fracture modeling - Theory, experimental investigation and numerical verification*. Ph.D. Thesis, Massachusetts Institute of Technology, 2007.
- [41] XUE L. Damage accumulation and fracture initiation in uncracked ductile solids subject to triaxial loading. *International Journal of Solids and Structures*, 2007, Vol. 44, Issue 16, pp. 5163–5181.
- [42] BAI Y., WIERZBICKI T. A new model of metal plasticity and fracture with pressure and Lode dependence. *International Journal of Plasticity*, 2008, Vol. 24, Issue 6, pp. 1071–1096.
- [43] XUE L. Stress based fracture envelope for damage plastic solids. *Engineering Fracture Mechanics*, 2009, Vol. 76, Issue 3, pp. 419–438.
- [44] BAI Y., WIERZBICKI T. Application of extended Mohr–Coulomb criterion to ductile fracture. *International Journal of Fracture*, 2010, Vol. 161, Issue 1, pp. 1–20.
- [45] LOU Y., HUH H., LIM S., PACK K. New ductile fracture criterion for prediction of fracture forming limit diagrams of sheet metals. *International Journal of Solids and Structures*, 2012, Vol. 49, Issue 25, pp. 3605–3615.
- [46] ZHOU J., GAO X., HAYDEN M., JOYCE J. A. Modeling the ductile fracture behavior of an aluminum alloy 5083-H116 including the residual stress effect. *Engineering Fracture Mechanics*, 2012, Vol. 85, pp. 103–116.
- [47] XUE Z., FALESKOG J., HUTCHINSON J. W. Tension–torsion fracture experiments – Part II: Simulations with the extended Gurson model and a ductile fracture criterion based on plastic strain. *International Journal of Solids and Structures*, 2013, Vol. 50, Issues 25–26, pp. 4258–4269.

- [48] KROON M., FALESKOG J. Numerical implementation of a J_2 - and J_3 -dependent plasticity model based on a spectral decomposition of the stress deviator. *Computational Mechanics*, 2013, Vol. 52, Issue 5, pp. 1059–1070.
- [49] LOU Y., HUH H. Extension of a shear-controlled ductile fracture model considering the stress triaxiality and the Lode parameter. *International Journal of Solids and Structures*, 2013, Vol. 50, Issue 2, pp. 447–455.
- [50] FABRÈGUE D., LANDRON C., BOUAZIZ O., MAIRE E. Damage evolution in TWIP and standard austenitic steel by means of 3D X ray tomography. *Materials Science and Engineering: A*, 2013, Vol. 579, pp. 92–98.
- [51] MALCHER L., REIS F. J. P., PIRES F. M. A., CÉSAR DE SÁ J. M. A. Evaluation of shear mechanisms and influence of the calibration point on the numerical results of the GTN model. *International Journal of Mechanical Sciences*, 2013, Vol. 75, pp. 407–422.
- [52] LOU Y., YOON J. W., HUH H. Modeling of shear ductile fracture considering a changeable cut-off value for stress triaxiality. *International Journal of Plasticity*, 2014, Vol. 54, pp. 56–80.
- [53] HŮLKA J. *Computational prediction of ductile fracture*. Ph.D. Thesis, Brno University of Technology, 2014 (in Czech).
- [54] ZHOU J., GAO X., SOBOTKA J. C., WEBLER B. A., COCKERAM B. V. On the extension of the Gurson-type porous plasticity models for prediction of ductile fracture under shear-dominated conditions. *International Journal of Solids and Structures*, 2014, Vol. 51, Issue 18, pp. 3273–3291.
- [55] ROTH CH. C., MOHR D. Effect of strain rate on ductile fracture initiation in advanced high strength steel sheets: Experiments and modeling. *International Journal of Plasticity*, 2014, Vol. 56, pp. 19–44.
- [56] GILIOLI A., MANES A., GIGLIO M., WIERZBICKI T. Predicting ballistic impact failure of aluminium 6061-T6 with the rate-independent Bao–Wierzbicki fracture model. *International Journal of Impact Engineering*, 2015, Vol. 76, pp. 207–220.
- [57] MARCADET S. J., MOHR D. Effect of compression–tension loading reversal on the strain to fracture of dual phase steel sheets. *International Journal of Plasticity*, 2015, Vol. 72, pp. 21–43.
- [58] PAPASIDERO J., DOQUET V., MOHR D. Ductile fracture of aluminum 2024-T351 under proportional and non-proportional multi-axial loading: Bao–Wierzbicki results revisited. *International Journal of Solids and Structures*, 2015, Vols. 69–70, pp. 459–474.
- [59] MOHR D., MARCADET S. J. Micromechanically-motivated phenomenological Hosford–Coulomb model for predicting ductile fracture initiation at low stress triaxialities. *International Journal of Solids and Structures*, 2015, Vols. 67–68, pp. 40–55.
- [60] KUBÍK P. *Implementation, calibration and application of ductile fracture conditions in FEM programs*. Ph.D. Thesis, Brno University of Technology, 2015 (in Czech).
- [61] TANCOCNE-DEJEAN T., ROTH CH. C., WOY U., MOHR D. Probabilistic fracture of Ti–6Al–4V made through additive layer manufacturing. *International Journal of Plasticity*, 2016, Vol. 78, pp. 145–172.

Curriculum vitæ

Personal details

Name	František Šebek
Date of birth	22. 05. 1988
Address	Krouna 316, 539 43 Krouna
E-mail	sebek@fme.vutbr.cz

Education

2012–to date	PhD, Brno University of Technology, Faculty of Mechanical Engineering, Institute of Solid Mechanics, Mechatronics and Biomechanics, programme Engineering Mechanics
2010–2012	Master's degree, Brno University of Technology, Faculty of Mechanical Engineering, Institute of Solid Mechanics, Mechatronics and Biomechanics, programme Engineering Mechanics and Biomechanics
2007–2010	Bachelor's degree, Brno University of Technology, Faculty of Mechanical Engineering, programme Mechanical Engineering
2003–2007	School-leaving examination, Secondary Industrial Technical School of Mechanical Engineering and Higher Vocational School Chrudim, programme Engineering

Career overview

2014–2015	Technician, Brno University of Technology, Faculty of Mechanical Engineering, Division of Virtual Modeling, Design and Testing, Section of Solid Mechanics, Mechatronics and Biomechanics
2015–to date	Researcher, Brno University of Technology, Faculty of Mechanical Engineering, Division of Virtual Modeling, Design and Testing, Section of Solid Mechanics, Mechatronics and Biomechanics

Languages

English	Level B2 (City & Guilds Level 1 Certificate in ESOL International (Spoken, reading, writing and listening): Communicator - B2, First Class Pass, 2014)
---------	--

Computer skills

ANSYS, Abaqus, MATLAB, Autodesk AutoCAD and Inventor, SolidWorks, Microsoft Word, Excel and PowerPoint, L^AT_EX

Abstract

This thesis is concerned with ductile fracture, which is a result of multiaxial quasi-static monotonic loading accompanied with large plastic deformations, while the local approach is considered for material degradation. In computations, the damage evolution is governed by used ductile fracture criteria. These were theoretically studied in the introduction, and the calibration procedure was proposed after the choice of suitable fracture criterion. Next, the experimental program was designed, and the tests on aluminium alloy 2024-T351, concerning tension, torsion and compression, were realized at a room temperature for the investigation of damage accumulation and reliable calibration of chosen phenomenological ductile fracture criterion, expressed through the fracture strain, and dependent on the hydrostatic pressure and deviatoric stress tensor. The ductile fracture model was then coupled with the yield criterion. Plasticity was considered in the form of taking into account the state of third invariant of deviatoric stress tensor as well for investigated material. The whole proposed approach that is fully applicable to multiaxial problems was implemented using user subroutine into the commercial software, based on the explicit finite element method. In the end, the application of the proposed approach to modelling of ductile fracture is presented in the form of verification using chosen specimens, resulting in the conclusions and recommendations for future studies.

Abstrakt

Práce se zabývá tvárným lomem, který je výsledkem víceosého kvazi-statického monotónního namáhání doprovázeného rozsáhlými plastickými deformacemi, přičemž pro degradaci materiálu je uvažován lokální přístup. Ve výpočtech o rozvoji poškození rozhodují použité mezní podmínky tvárného lomu. Tyto byly teoreticky studovány v úvodu práce a po výběru vhodné mezní podmínky byl stanoven postup kalibrace. Dále byl rozpracován plán měření a realizovány zkoušky při pokojové teplotě na slitině hliníku 2024-T351, zahrnující tah, krut a tlak, pro studium rozvoje poškození a věrohodnou kalibraci vybraného fenomenologického modelu tvárného porušování, vyjádřeného pomocí lomového přetvoření a závislého na hydrostatickém tlaku a deviátoru tenzoru napětí. Mezní podmínka tvárného lomu byla posléze svázána s podmínkou plasticity. Plasticita byla pro zkoumaný materiál uvažována ve tvaru zohledňujícím i stav třetího invariantu deviátoru tenzoru napětí. Celý navržený přístup, plně aplikovatelný na víceosé úlohy, byl implementován pomocí uživatelské rutiny do komerčního programu založeného na explicitní variantě metody konečných prvků. V závěru práce je předložena aplikace navrženého přístupu k modelování tvárného porušování v podobě verifikace na vybraných zkušebních testech, z níž plynou závěry a doporučení pro další práci.